Science of the Total Environment 858 (2023) 159657

Contents lists available at ScienceDirect

Science of the Total Environment

journal homepage: www.elsevier.com/locate/scitotenv

Impact of urban aerosols on the cloud condensation activity using a clustering model

Fernando Rejano [a,b,*], Juan Andrés Casquero-Vera [c,a,b,**], Hassan Lyamani [d], Elisabeth Andrews [e,f], Andrea Casans [a,b], Daniel Pérez-Ramírez [a,b], Lucas Alados-Arboledas [a,b], Gloria Titos [a,b], Francisco José Olmo [a,b]

[a] Andalusian Institute for Earth System Research, IISTA-CEAMA, University of Granada, Junta de Andalucía, Granada 18006, Spain
[b] Department of Applied Physics, University of Granada, Granada 18071, Spain
[c] Institute for Atmospheric and Earth System Research (INAR)/Physics, Faculty of Science, University of Helsinki, Helsinki, Finland
[d] Applied Physics I Department, University of Malaga, Malaga 29071, Spain
[e] Cooperative Institute for Research in Environmental Sciences, University of Colorado, Boulder, CO 80309, United States
[f] Earth System Research Laboratory, National Oceanic and Atmospheric Administration, Boulder, CO 80305, United States

HIGHLIGHTS

- This study aims to explore the influence of different urban aerosol populations in the CCN properties.
- Five main aerosol categories were identified using k-means clustering.
- Urban background and aged traffic are the most efficient CCN categories.
- Despite particles from traffic emissions are not efficient CCN, these particles can undergo ageing and affect cloud formation.

GRAPHICAL ABSTRACT

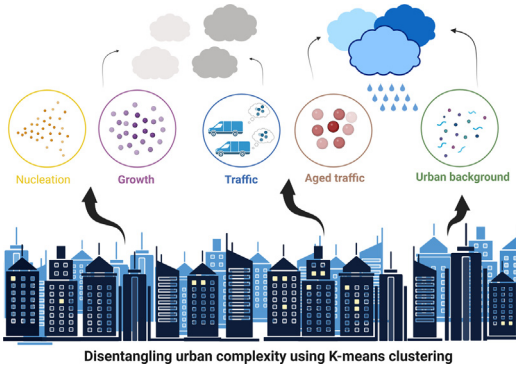

ARTICLE INFO

Editor: Hai Guo

Keywords:
Activation properties
CCN
Particle size distribution
K-means clustering

ABSTRACT

The indirect effect of aerosols on climate through aerosol-cloud-interactions is still highly uncertain and limits our ability to assess anthropogenic climate change. The foundation of this uncertainty is in the number of cloud condensation nuclei (CCN), which itself mainly stems from uncertainty in aerosol sources and how particles evolve to become effective CCN. We analyze particle number size distribution (PNSD) and CCN measurements from an urban site in a two-step method: (1) we use an unsupervised clustering model to classify the main aerosol categories and processes occurring in the urban atmosphere and (2) we explore the influence of the identified aerosol populations on the CCN properties. According to the physical properties of each cluster, its diurnal timing, and additional air quality parameters, the clusters are grouped into five main aerosol categories: nucleation, growth, traffic, aged traffic, and urban background. The results show that, despite aged traffic and urban background categories are those with lower total particle number concentrations (N_{tot}) these categories are the most efficient sources in terms of contribution to the overall CCN budget with activation fractions (AF) around 0.5 at 0.75 % supersaturation (SS). By contrast, road traffic is an important aerosol source with the highest frequency of occurrence (32 %) and relatively high N_{tot}, however, its impact in the CCN activity is very limited likely due to lower particle mean diameter and hydrophobic chemical composition. Similarly, nucleation and growth categories, associated to new particle formation (NPF) events, present large N_{tot} with large frequency of occurrence (22 % and 28 %, respectively) but the CCN concentration for these categories is about half of the CCN concentration observed for the aged traffic

* Correspondence to: F. Rejano, Andalusian Institute for Earth System Research, IISTA-CEAMA, University of Granada, Junta de Andalucía, Granada 18006, Spain.
** Correspondence to: J.A. Casquero-Vera, Institute for Atmospheric and Earth System Research (INAR)/Physics, Faculty of Science, University of Helsinki, Helsinki, Finland.
E-mail addresses: frejano@ugr.es (F. Rejano), juan.casquero@helsinki.fi (J.A. Casquero-Vera).

http://dx.doi.org/10.1016/j.scitotenv.2022.159657
Received 15 July 2022; Received in revised form 19 October 2022; Accepted 19 October 2022
Available online 25 October 2022
0048-9697/© 2022 The Authors. Published by Elsevier B.V. This is an open access article under the CC BY license (http://creativecommons.org/licenses/by/4.0/).

category, which is associated with their small size. Overall, our results show that direct influence of traffic emissions on the CCN budget is limited, however, when these particles undergo ageing processes, they have a significant influence on the CCN concentrations and may be an important CCN source. Thus, aged traffic particles could be transported to other environments where clouds form, triggering a plausible indirect effect of traffic emissions on aerosol-cloud interactions and consequently contributing to climate change.

1. Introduction

Estimating and constraining anthropogenic radiative forcing is one of the most important challenges in atmospheric science and it is crucial to understand and mitigate climate change (Intergovernmental Panel on Climate Change (IPCC), 2021). The indirect aerosol radiative forcing through aerosol-cloud-interactions (ACI) is the most uncertain component of the anthropogenic forcing (Seinfeld et al., 2016). This is due to the complexity of the processes related to the activation of aerosol particles as cloud condensation nuclei (CCN). Aerosol particles that can become cloud droplets can affect cloud properties depending on their concentration in the atmosphere and their physicochemical properties (Crosbie et al., 2015; Paramonov et al., 2015; Schmale et al., 2018). Therefore, it is important to identify (i) the aerosol sources that may contribute to CCN concentration and (ii) how particles evolve in the atmosphere to become effective CCN. Assessing the importance of anthropogenic sources in the CCN budget is crucial to estimate/constrain the anthropogenic radiative forcing through ACI.

The particle number size distribution (PNSD) is a key property of an aerosol particle population that provides valuable insights into the formation, transformation and removal processes of particles and the potential aerosol sources (Beddows et al., 2009; Rivas et al., 2020). Analyzing the shape of the PNSD makes possible to identify atmospheric aerosol sources (Brines et al., 2015; Charron et al., 2008; Costabile et al., 2009; Salimi et al., 2014), while the temporal evolution of the PNSD makes possible to observe atmospheric processes such as nucleation, coagulation, condensation and/or deposition (Tunved et al., 2004). To assess the impact on climate and health of the large variety of aerosol sources and processes, several PNSD source apportionment methods have been developed and used to identify aerosol sources (e.g., Beddows et al., 2009, 2015; Cai et al., 2020; Casquero-Vera et al., 2021; Rivas et al., 2020; Rodríguez and Cuevas, 2007). When the aerosol sources are well known, positive matrix factorization (PMF) or non-positive matrix factorization (NPMF) methods can determine the contribution of each source to the aerosol population (Crilley et al., 2017; Liang et al., 2021; Rivas et al., 2020). However, when aerosol sources are not known, clustering methods enable the identification of aerosol population types in terms of statistical similarities which can be related to sources or atmospheric processes (Atwood et al., 2019; Beddows et al., 2009; Brines et al., 2014, 2015; Costabile et al., 2009; Ripamonti et al., 2013; Salimi et al., 2014; Tunved et al., 2004). This unsupervised machine-learning method has been performed satisfactorily in a wide variety of environments which are affected by different sources or processes such as marine sites (Atwood et al., 2017, 2019), rural sites (Beddows et al., 2009; Charron et al., 2008; Lee et al., 2021) and urban sites (Agudelo-Castañeda et al., 2019; Brines et al., 2014, 2015; Wegner et al., 2012). Among all sites, urban areas are the most interesting sites to be explored using clustering methods due to the high number of aerosol sources influenced by anthropogenic activity (traffic, industry, biomass burning or domestic heating systems) and the complex atmospheric processes which takes place (Wu and Boor, 2021).

Additionally to the aforementioned information provided by PNSD, it is important to bear in mind that particle size is the most critical factor controlling the activation of aerosol particles as CCN (Andreae and Rosenfeld, 2008; Atwood et al., 2019; Dusek et al., 2006; Rejano et al., 2021), being the effect of aerosol chemical composition less important (Schmale et al., 2018). In this sense, several studies analyzed the activation properties of aerosols as CCN in relation to the PNSD (e.g., Bougiatioti et al., 2020; Cheung et al., 2020), but there is still a lack of knowledge about the sources' contributions to the CCN budget. Disentangling the influence of the different aerosol populations in the CCN properties is complicated since some sources or process may mask others, even more in urban areas where the complexity is higher. Clustering techniques applied to PNSD data are a promising tool to explore the influence of a specific aerosol source or physicochemical process on the CCN concentration. Thus, this study aims to understand the impact of the different aerosol categories in the CCN concentrations and activation properties by using k-means clustering analysis.

To this end, in this study we investigate concurrent PNSD measurements in a wide size range (4–500 nm) and CCN concentrations at an urban background site in south-eastern Spain. We perform a clustering analysis of the PNSD data to identify the most common aerosol populations. Including sub-10 nm measurements in the clustering analysis allows for a better understanding of atmospheric processes in urban environments. Then we investigate the activation properties of each aerosol population to determine their influence in the overall CCN concentrations.

2. Measurements and methods

2.1. Sampling site

The study was carried out in south-eastern Spain at the Andalusian Global Observatory of the Atmosphere (AGORA) covering the period from 15 of April to 1 of November of 2020. The experimental station (UGR) is at the Andalusian Institute for Earth System Research (IISTA-CEAMA), an urban background station located in the city of Granada, Spain (37.18°N, 3.58°W, 680 m a.s.l.). This station is part of ACTRIS (Aerosol, Cloud and Trace gases Research Infrastructure, http://actris.eu) (Pandolfi et al., 2018; Rose et al., 2021) and is included in the NOAA Federated Aerosol Network, NFAN (Andrews et al., 2019).

Granada is a medium-size city with a population of 231.775, which increases up to 541.465 if the whole metropolitan area is considered (www.ine.es, 2020). The city is situated in a natural basin surrounded by mountains with elevations between 1000 and 3479 m a.s.l. Granada is a non-industrialized city but it is one of the Spanish cities that suffers from pollution problems (Casquero-Vera et al., 2019). The main local aerosol source is road traffic, including both motor vehicle exhaust and resuspension of particulate material from the roadways (Titos et al., 2014). In winter, domestic heating and biomass burning for agricultural waste removal are additional sources of anthropogenic pollution (Casquero-Vera et al., 2022; Titos et al., 2017). Moreover, the orography of Granada favors winter temperature inversions and predominance of very weak wind speeds, which can lead to a large accumulation of particles near the surface (Lyamani et al., 2012) and may cause environmental and human health problems. The major external aerosol source affecting the study area is Saharan dust from North Africa (Lyamani et al., 2005; Pérez-Ramírez et al., 2016; Valenzuela et al., 2012).

2.2. Instrumentation

The PNSD was measured in the diameter range between 4 and 500 nm with a size-bin resolution of 64 channels per decade and a temporal resolution of 5 min by using a SMPS (Scanning Mobility Particle Size spectrometer) and nano-SMPS (TSI model 3938). Both SMPS systems consist of an electrostatic classifier (TSI 3082), a differential mobility analyzer (DMA; TSI 3081 for SMPS and TSI 3085 for nano-SMPS) and a condensation particle counter (CPC; TSI 3772 and TSI 3775, respectively). The aerosol flow rates for the SMPS and nano-SMPS were 1.0 and 1.5 lpm, respectively,

and sheath flow was 5 lpm for both systems. The quality of the SMPS measurements was assured by frequently checking the flow rates, performing 203 nm PSL calibrations and with in-situ intercomparison (ACTRIS Round Robin Tour), following the ACTRIS and GAW recommendations (Wiedensohler et al., 2012).

Polydisperse CCN measurements were performed using a DMT cloud condensation nuclei counter (CCNc) model CCN-100. The CCNc measured the CCN concentration at three SS values: 0.25, 0.50 and 0.75 %, taking 15 min at each SS value. To ensure data quality due to instabilities of the SS value in the growth chamber, the instrument data was filtered according to Rejano et al. (2021) criteria. It consists of a two-step filtering process that first removes all data above 1st percentile and below 99th and afterwards removes all data whose SS values differ >20 % from the setpoint value. The total flow rate of the instrument was fixed at 0.5 lpm with an aerosol to total flow ratio of 10. The flow rates were checked frequently during the measurement period and SS calibration was done at the beginning and the end of the measurement period following ACTRIS guidelines (http://actris.nilu.no/Content/SOP).

Some additional atmospheric parameters were measured as explanatory variables for the aerosol classification. The equivalent black carbon (eBC) mass concentration has been recognized as a proxy of traffic emissions for this urban site (Lyamani et al., 2011). The eBC concentration was measured using a Multi-Angle Absorption Photometer (MAAP, Thermo Scientific model 5012) with 1 min resolution. This filter-based instrument infers the eBC concentration from the aerosol absorption coefficient (σ_{ap}) at 637 nm assuming a mass absorption cross section of 6.6 $m^2\ g^{-1}$ (Müller et al., 2011). O_3 concentration is considered a good proxy of photochemical NPF in high insolation urban areas (Brines et al., 2015). The O_3 concentration data with time resolution of 10 min was obtained from a nearby air quality station. O_3 data are provided by the regional government (Junta de Andalucía, http://www.juntadeandalucia.es/medioambiente) following the requirements of the European air quality directives. This air quality station is about ~500 m away from UGR station, and previous studies have shown that both sites are exposed to similar atmospheric conditions and aerosol sources (Titos et al., 2015).

3. Data analysis and methods

3.1. K-means clustering analysis

The clustering technique is commonly used in atmospheric sciences to divide data into different groups with similar properties and therefore reduce data complexity. The k-means clustering technique consists of an unsupervised machine learning method that separates data into *k* groups, minimizing a criterion known as the inertia or within-cluster-sum-of-squares (Wilks, 2019). All clusters are associated with a centroid, which is defined as the location representing the centre of the cluster. Therefore, each data point is allocated to the cluster that presents the minimum distance between this data point and the cluster centroid. This method requires a set of variables that define the position of each sample and the cluster centroids. Since the k-means algorithm is an iterative process, the final clustering classification may show some dependence on the initial values of the centroid positions. To avoid the initial condition effect on the k-means clustering solution, the clustering was repeated 10 times using new initial centroid positions each time.

In our analysis the PNSD across 137 size bins (spanning the size range from 4 nm up to 500 nm) was selected as input for the k-means clustering analysis. All PNSD used are normalized by the maximum of the PNSD because the shape of the PNSD is related to specific aerosol sources or origin, whereas the absolute values of PNSD might be also influenced by temporal variability along the measurement period.

3.2. Determination of optimal number of clusters

The results obtained by clustering algorithms depend on the selection of the number of clusters, requiring an a priori specification of the optimum number of clusters. The validation of the results obtained by clustering algorithms as well as the optimum number of clusters is a fundamental part of the clustering process. The most common approaches for cluster validation are based on internal cluster validity indices which allow identification of dense and well-separated clusters. In this study, the Davies-Bouldin index (DB) was calculated for the cluster solution ranging from 3 to 15 clusters. The DB criterion is based on a ratio of within-cluster and inter-cluster distances with the optimal clustering solution having the smallest DB index value (Davies and Bouldin, 1979). Our choice of the DB criteria is based on: i) Arbelaitz et al. (2013) analysis, which performed an extensive comparative study of the performance of 30 clustering validation indices and identified the DB index as one of the best performing indices, and ii) the computation of the DB index requires less computational time than other validation indices.

Fig. 1 shows the DB index values for each clustering solution. Two clear minima are observed for the solutions of 5 and 10 clusters, indicating that these two configurations are the best solutions offering well-defined and separated clusters. The clustering solution with ten clusters shows a lower DB value than the five clusters solution (DB index values are 1.403 and 1.411, respectively). Despite the small difference, we selected the 10-cluster solution to reduce the possibility that any cluster included PNSDs from various sources/processes. Afterwards, based on the scientific context, these 10 clusters will be grouped into five main aerosol categories as recommended in the literature (Brines et al., 2014; Dall'Osto et al., 2011), to study their activation capacity as CCN as described in Section 4.1 of the results.

3.3. Effective activation parameters from CCN measurements

In the case of polydisperse CCN measurements, the effective critical diameter (D_{crit}) is defined as the diameter above which all aerosol particles are activated. The effective D_{crit} can be calculated by considering both the measured PNSD and the CCN measurements at a fixed SS value (N_{CCN} (SS)) and assuming a sharp activation cut-off (Jurányi et al., 2011):

$$N_{CCN}(SS) = \int_{D_{crit}(SS)}^{D_{max}} \frac{dN}{dlogD_p} dlogD_p \quad (1)$$

where D_p is the particle diameter and D_{max} is the upper limit of the PNSD. The particle number size distribution is integrated from its upper limit to the diameter at which the integral value equals the simultaneously

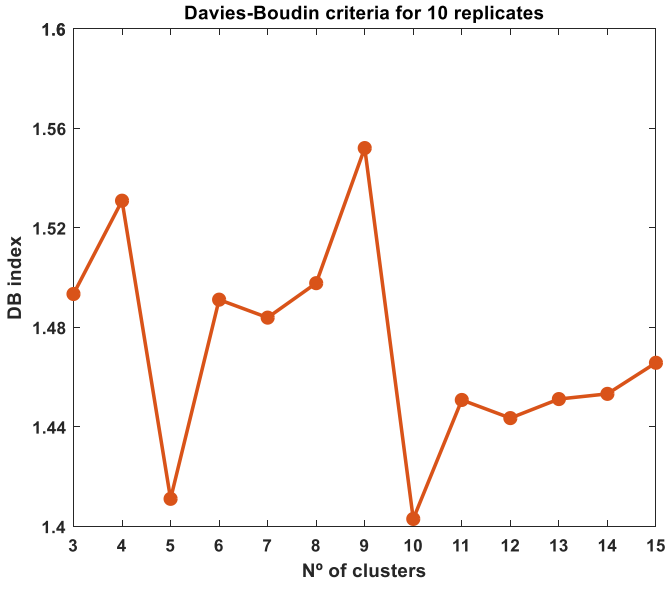

Fig. 1. Mean Davies-Bouldin (DB) index values for each number of cluster solutions. Each data point is the averaged value for the 10 different replicates of the initial position of centroids.

measured N_{CCN}(SS). The total particle number concentration (N_{tot}) is computed integrating the whole PNSD and used to calculate the activation fraction (AF) as the ratio N_{CCN}/N_{tot}.

The hygroscopicity parameter is a parameterization of aerosol hygroscopicity which is related to the chemical composition of a specific aerosol particle (Petters and Kreidenweis, 2007). However, it is very common to retrieve an effective hygroscopicity parameter (κ from now on) for the whole population of aerosol particles. The effective hygroscopicity parameter can be retrieved using κ-Köhler theory from aerosol size distribution and CCN measurements (Jurányi et al., 2011; Rejano et al., 2021; Salma et al., 2021). This method uses the D_{crit}(SS) obtained from Eq. (1) as the dry diameter in the Köhler curve. In this way, the corresponding κ value is the one that equals the critical SS for this Köhler curve to the instrument SS. Further information on the methodology can be found in Rejano et al. (2021) and references therein. These CCN-derived κ values quantify the effective hygroscopicity of activated particles in the CCNc and show a dependence on SS. Thus, the effective κ parameter gives information about a certain particle size range depending on the SS value. For example, at low SS values κ would describe the hygroscopicity of accumulation mode particles (Salma et al., 2021).

4. Results and discussion

In this section, we present the classification of the PNSD dataset based on the cluster analysis and the identification of the sources and processes related to each cluster. Then, the resulting clusters are grouped into main aerosol population types according to some explanatory parameters. Finally, the CCN activity of each aerosol population is obtained to quantify and compare the impact of each aerosol category in the CCN properties.

4.1. Aerosol classification by cluster analysis

We apply the k-means clustering analysis to the data matrix that consists of 48.441 measurements of 5-min resolution PNSD with 137 diameter size bins (from 4 to 500 nm). According to the criteria explained in Section 3.2, the analysis has been performed with a fixed output of 10-clusters. Fig. 2 shows the mean normalized PNSD associated with each cluster resulting from the k-means clustering analysis. According to their frequency of occurrence (diurnal and monthly, Fig. S1) and their relationship with other atmospheric constituents such as eBC and ozone and having analyzed the clustering solution within the scientific context of previous aerosol studies performed in this site (del Águila et al., 2018; Casquero-Vera et al., 2021; Titos et al., 2014, 2017), we regrouped the 10 clusters into 5 aerosol categories. The reduction of the cluster solution to a more generic classification based on existing knowledge of PNSDs observed has been widely used in the bibliography (Agudelo-Castañeda et al., 2019; Brines et al., 2014, 2015; Dall'Osto et al., 2011; Salimi et al., 2014). Table 1 summarizes the main characteristics of each of the five categories (also for the whole measurement period) including their frequency of occurrence, the diameter where the maximum of the PNSD is found, the total particle number concentration, eBC and ozone concentrations. To ensure that differences between mean values of those variables associated to each category (particle concentration, ozone and eBC concentrations) are statistically significant, we have performed an analysis of variance test (Kruskal and Wallis test, which is a non-parametric version of one-way ANOVA; Kruskal and Wallis, 1952) for those variables, in order to check if the means values of each category are significatively different. The result of Kruskal and Wallis test showed *p*-values $<10^{-4}$, therefore the differences between the tested groups are statistically significant. Below, we describe the five main categories and the clusters included in each one:

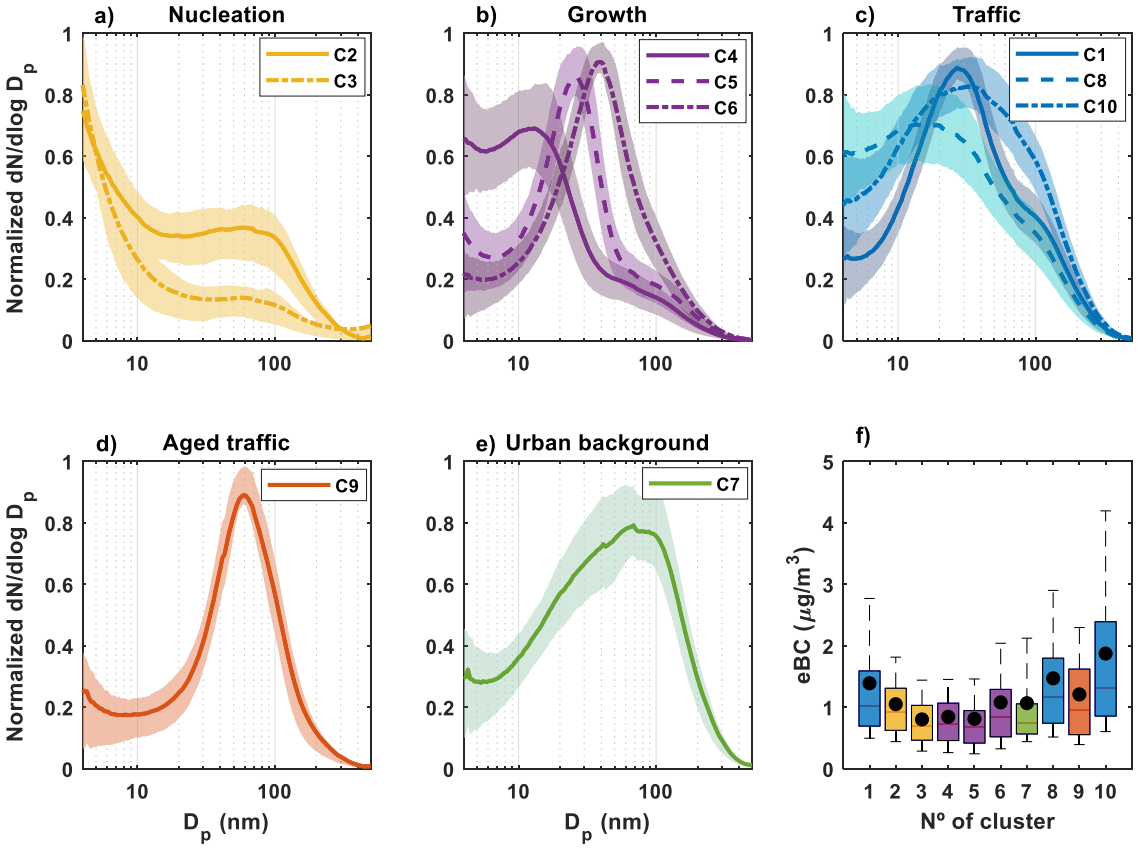

Fig. 2. Mean normalized PNSD for each cluster. The shaded area represents the interquartile distance (percentile 25th–75th). The 10 clusters are colored according to the aerosol population classification. The right bottom subplot shows the equivalent black carbon (eBC) concentration boxplot for each cluster. The black dots represent the mean value.

Table 1
Mean aerosol properties (± standard deviation, STD) for each category and for the whole measurement period.

Aerosol category	N_{tot} ($\cdot 10^4$ cm^{-3})	Maximum of the PNSD (nm)	eBC (μg/m^3)	O_3 (μg/m^3)	Frequency of occurrence (%)
Nucleation	1.5 ± 1.2	4	0.9 ± 0.6	65 ± 26	22
Growth	1.4 ± 1.0	23	0.9 ± 0.7	68 ± 25	28
Traffic	1.2 ± 0.7	27	1.6 ± 1.3	61 ± 23	32
Aged traffic	1.1 ± 0.7	60	1.2 ± 0.9	48 ± 22	8
Urban background	0.7 ± 0.4	70	1.1 ± 0.9	59 ± 25	10
Whole period	1.2 ± 0.9	26	1.2 ± 1.0	63 ± 26	100

- *Nucleation*: This category includes clusters 2 and 3 (Fig. 2a), both characterized by significant contribution of nucleation mode (<25 nm) particles and similar PNSD shape, exhibiting the PNSD maximum at 4 nm. These clusters occur more frequently during the period from June–August (Fig. S1a and S1f) and predominantly at midday. The PNSDs of clusters 2 and 3, together with their frequent occurrence during summer, suggest that these clusters can be associated with freshly nucleated particles during new particle formation (NPF) events that have been previously observed mainly during warm periods at this site (Casquero-Vera et al., 2021). This category represents the 22 % of the dataset and show high N_{tot} (cluster 3 has N_{tot} ~20.000 cm^{-3} and cluster 2 ~10.000 cm^{-3}), higher O_3 concentration and lower eBC concentration respect to the averaged value for the whole period (Table 1). The high total particle number concentration is mainly driven by the nucleation mode that constitutes 67 % of the total particle concentration of this category as it is observed during NPF events in previous studies (Casquero-Vera et al., 2020).

- *Growth*: This category includes clusters 4, 5 and 6 that are characterized by PNSD with maxima at 12, 26 and 40 nm, respectively. Each of these clusters represent a different stage of particles growing from smaller sizes. These clusters show a clear relationship with the nucleation clusters as they have low eBC and high O_3 concentrations (Table 1) as well. This category represents the 28 % of the dataset, similar to the nucleation category. These clusters occur more frequently during warm months when NPF events are more frequent, in coincidence with occurrence of the nucleation clusters (Fig. S1b, S1g and S1i). Cluster 4 occurs more frequently between 11:00–13:00 UTC, 2 h later than the nucleation clusters, representing the first stage of growth after NPF events. Freshly nucleated particles grow from ~4 nm (clusters 2–3) to ~12 nm (cluster 4) over approximately a two-hour period. This growth corresponds to a growth rate of ~4 nm·h^{-1} which is in the range of growth rates previously observed in the study area (Casquero-Vera et al., 2020). Cluster 5 represents the second stage of particle growth with the PNSD maximum situated at larger sizes and lower total particle number concentration than cluster 4 (N_{tot} ~12.000 cm^{-3}), while cluster 6 represents the last stage of the particle growth with the PNSD maximum at 40 nm and shows the lowest total particle number concentration of the growth category (N_{tot} ~10,000 cm^{-3}). This cluster has its highest frequency of occurrence around 20:00 UTC, especially in summer (Fig. S1i). At this time of the day, traffic emissions might also influence the observed PNSDs as confirmed by the slightly higher eBC concentration observed for this cluster (Fig. 2f). This explanation of particle growth from the nucleation mode to larger sizes is consistent with previous studies in Granada urban area during NPF events where particle growth rates between 4 and 7 nm ($GR_{4–7}$) and 7 and 25 nm ($GR_{7–25}$) were 3.6 ± 0.8 nm h^{-1} and 4.5 ± 1.0 nm h^{-1}, respectively (Casquero-Vera et al., 2020).
- *Traffic*: This category comprises the PNSDs associated with clusters 1, 8 and 10, and represents 32 % of the data. These clusters show wider size distributions covering the diameter range from nucleation to accumulation mode particles (Fig. 2c). Their PNSDs have maximums located at 28, 17 and 37 nm, respectively. The total particle number concentration of these clusters is very similar, with mean N_{tot} around 12.000 cm^{-3} (Table 1). However, the key to associate this category with traffic emissions are the statistically significant higher concentration of eBC (Fig. 2f) and the marked diurnal frequency of occurrence with two peaks (Fig. S1c, S1h, S1j) in coincidence with the diurnal cycle of eBC (Fig. S2, 7:00–8:00 UTC morning peak and 19:00–20:00 UTC evening peak). Cluster 10 has its maximum occurrence during the morning traffic peak (around 7:00 UTC) while cluster 8 has its maximum during evening peak (around 19:00 UTC). Differences between these two clusters are the larger eBC of cluster 10 (1.87 μg/m^3, being the cluster with the highest mean eBC concentration) and the difference in the nucleation mode sizes with higher contribution in cluster 8. Also, previous studies in this site pointed out that traffic is one of the most important sources of sub-micron particles and the observed diurnal pattern agree with our results (del Águila et al., 2018; Casquero-Vera et al., 2021).
- *Aged traffic:* This category only includes cluster 9 and represents only the 8 % of the dataset. The PNSD maximum occurs at 60 nm (Fig. 2d) and N_{tot} is around 11,000 cm^{-3}. This cluster shows, after traffic category, the highest eBC concentrations, the lowest ozone concentration and occurs mainly between 9:00–10:00 UTC (Fig. S1d), 2 h after the traffic morning peak (Fig. S2). This cluster is slightly delayed from morning traffic rush hours and with larger particles than fresh traffic particles was identified in other urban site and also was referred as aged traffic (Agudelo-Castañeda et al., 2019). It is known that volatile gaseous compounds emitted by traffic can undergo photochemical processes to produce less volatile species, which can promote secondary aerosol formation via condensation (Gentner et al., 2012; Robinson et al., 2007; Rönkkö et al., 2017). This complex chemical process involves some oxidation reactions that might require O_3 to occur (Kroll and Seinfeld, 2008), which is consistent to the fact that this cluster has the lowest O_3 concentration of all clusters (Table 1). Therefore, we suggest this ageing pathway as a plausible process affecting these particles.
- *Urban background*: This category is composed of cluster 7 with a frequency of occurrence of 10 % over the study period. Mean PNSD of this category shows a maximum at 70 nm (Fig. 2e) and the N_{tot} is around 7.000 cm^{-3}, which are the largest diameter and the lowest concentration of all categories (Table 1). The low values of eBC (mean of 1.1 μg/m^3) suggest low influence of traffic emissions. Also, cluster 7 occurs normally during night-time when anthropogenic emissions are considerably reduced in the study area (Fig. S1e). This fact explains the low N_{tot} of this cluster and, together with the maximum of the PNSD located at 70 nm, suggest that this cluster is associated with urban background aerosol. In this sense, similar characteristics of urban background aerosol has been reported previously by Brines et al. (2015) in three different urban sites (Madrid, Barcelona, and Brisbane) with maximum of the PNSD located between 60 and 70 nm. This category was observed at this site during different measurements periods (del Águila et al., 2018). Furthermore, the associated eBC concentrations support our observations.

Once we have identified the main aerosol categories in the diameter range between 4 and 500 nm at this site (see the corresponding PNSD for each category in Fig. 3), we observe that traffic and growth categories are the most important categories in terms of its observation frequency (32 % and 28 %, respectively) (Table 1). Also, we point out that during the analyzed period the PNSD is mainly controlled by traffic emissions and NPF events, including freshly nucleated particles and first stage growth

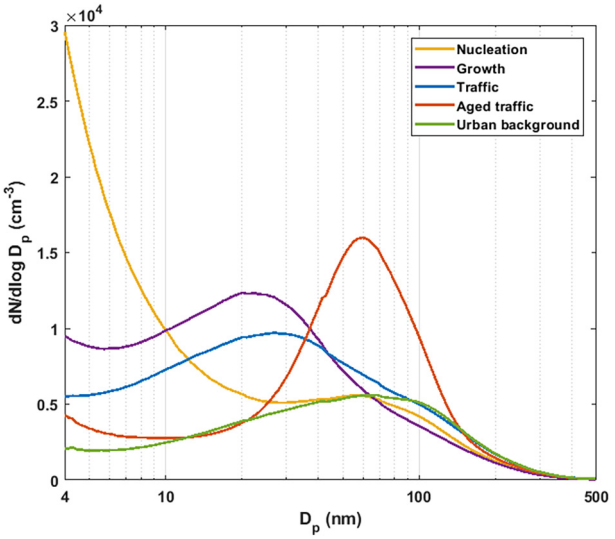

Fig. 3. Mean PNSD of each aerosol population type.

particles, representing the 82 % of dataset. The five main aerosol categories that we have identified are consistent with previous studies dealing with identification of submicron aerosols sources (del Águila et al., 2018; Casquero-Vera et al., 2020, 2021; Rejano et al., 2021). Despite previous studies in this site observed other aerosol sources such as domestic heating or biomass burning (Casquero-Vera et al., 2021; Titos et al., 2017), we could not identify these aerosol sources since the measurement period lasted until November, when those sources are not activated yet. We realized that traffic influence on the PNSD is not limited to fresh emissions since an indirect influence has been observed due to the ageing of these particles. However, it shows a limited influence in the aerosol population (just an 8 % of frequency of occurrence). The retrieved aerosol categories reflect the impact of the multiple urban aerosol sources on the PNSD, which in turn would lead to differences in the chemical composition. These differences could result in differences in the aerosol activation properties as CCN, and therefore, different effects on cloud formation and climate.

4.2. CCN properties associated with each aerosol category

Based on the previous aerosol classification by cluster analysis, in this section we investigate their relationships with coincident polydisperse CCN measurements at three supersaturation values (SS = 0.25, 0.50 and 0.75 %). The following activation parameters are investigated for the different aerosol categories: CCN concentration (N_{CCN}), activation fraction (AF), critical diameter (D_{crit}) and hygroscopicity parameter (κ). Table 2 shows the mean and standard deviation of the activation parameters for the three SS associated with each aerosol category. Also, Fig. 5 presents the box-whisker plot for these parameters (N_{CCN}, AF, D_{crit} and κ) for the three SS values. A general comparison of each activation parameter and its differences between the main aerosol categories is discussed below. As in Section 4.1, in order to check if the differences between the mean values for the different aerosol categories are statically significant, we have performed the Kruskal and Wallis test for all activation parameters associated to each aerosol category. Results of the test showed *p*-values $<10^{-4}$, which mean that the observed differences are statistically significant.

4.2.1. CCN concentration (N_{CCN})

The mean CCN concentration in this study ranges from 1.000 to 2.000 cm^{-3} at SS = 0.25 % and from 1.900 to 4.600 at SS = 0.75 %. The aged traffic category clearly shows the highest values for all SS values, while the other categories present more similar values, being growth category the one with the lowest N_{CCN} values. All aerosol categories, except aged traffic, exhibit similar mean N_{CCN} values, around 1200 cm^{-3}, due to their similar PNSD shape in the accumulation size range (between 100 and 500 nm, see Fig. 3). The urban background category presents a bit higher concentration than nucleation, growth, and traffic (Table 2). According to N_{CCN} variability represented by the box and whisker size, aged traffic category shows much more variability than the other categories (Fig. 4). As the SS value increases all CCN concentrations become higher since smaller particles can activate as CCN (Fig. 4). However, not all aerosol categories do so in the same way. The nucleation, growth, traffic, and urban background categories increase their concentrations by approximately 600 cm^{-3} when SS increases from 0.25 % to 0.50 %; whereas for the same SS change the aged traffic category increases its concentration by 1600 cm^{-3} (Table 2).

Table 2
Overview of activation properties at different supersaturation (mean value ± standard deviation) for each aerosol population and for the whole measurement period. The median value for each variable is also included between parenthesis.

SS (%)	Parameter	Aerosol category					
		Nucleation	Growth	Traffic	Aged Traffic	Urban background	Whole period
0.25	N_{CCN} ($\cdot 10^3$ cm^{-3})	1.2 ± 0.7 (1.1)	1.0 ± 0.6 (0.9)	1.1 ± 0.5 (1.1)	2.0 ± 1.5 (1.5)	1.3 ± 0.5 (1.3)	1.2 ± 0.5 (1.1)
	AF (−)	0.18 ± 0.09 (0.17)	0.11 ± 0.06 (0.10)	0.15 ± 0.06 (0.14)	0.23 ± 0.09 (0.22)	0.26 ± 0.08 (0.26)	0.16 ± 0.09 (0.15)
	D_{crit} (nm)	96 ± 13 (95)	97 ± 13 (95)	103 ± 15 (102)	90 ± 11 (91)	96 ± 10 (95)	98 ± 14 (98)
	κ (−)	0.25 ± 0.10 (0.24)	0.24 ± 0.10 (0.24)	0.20 ± 0.09 (0.20)	0.30 ± 0.11 (0.27)	0.25 ± 0.10 (0.24)	0.24 ± 0.10 (0.22)
0.50	N_{CCN} ($\cdot 10^3$ cm^{-3})	1.8 ± 1.2 (1.7)	1.5 ± 0.9 (1.4)	1.7 ± 0.7 (1.6)	3.6 ± 2.5 (2.6)	2.0 ± 0.7 (1.8)	1.9 ± 1.3 (1.7)
	AF (−)	0.28 ± 0.13 (0.26)	0.17 ± 0.08 (0.16)	0.22 ± 0.08 (0.21)	0.41 ± 0.11 (0.40)	0.39 ± 0.09 (0.38)	0.25 ± 0.13 (0.23)
	D_{crit} (nm)	71 ± 13 (69)	70 ± 11 (69)	77 ± 14 (76)	66 ± 14 (66)	70 ± 9 (71)	72 ± 13 (71)
	κ (−)	0.18 ± 0.09 (0.17)	0.18 ± 0.09 (0.17)	0.14 ± 0.08 (0.12)	0.20 ± 0.09 (0.19)	0.17 ± 0.06 (0.15)	0.17 ± 0.09 (0.15)
0.75	N_{CCN} ($\cdot 10^3$ cm^{-3})	2.4 ± 1.5 (2.1)	1.9 ± 1.0 (1.8)	2.1 ± 1.0 (2.0)	4.6 ± 3.0 (3.3)	2.3 ± 1.0 (2.1)	2.4 ± 1.6 (2.0)
	AF (−)	0.34 ± 0.14 (0.34)	0.22 ± 0.09 (0.21)	0.29 ± 0.08 (0.29)	0.51 ± 0.10 (0.50)	0.46 ± 0.08 (0.46)	0.32 ± 0.14 (0.31)
	D_{crit} (nm)	57 ± 8 (57)	56 ± 7 (55)	60 ± 9 (59)	56 ± 6 (55)	58 ± 6 (57)	57 ± 8 (57)
	κ (−)	0.15 ± 0.09 (0.13)	0.15 ± 0.07 (0.14)	0.12 ± 0.06 (0.12)	0.15 ± 0.07 (0.14)	0.13 ± 0.05 (0.13)	0.14 ± 0.07 (0.13)

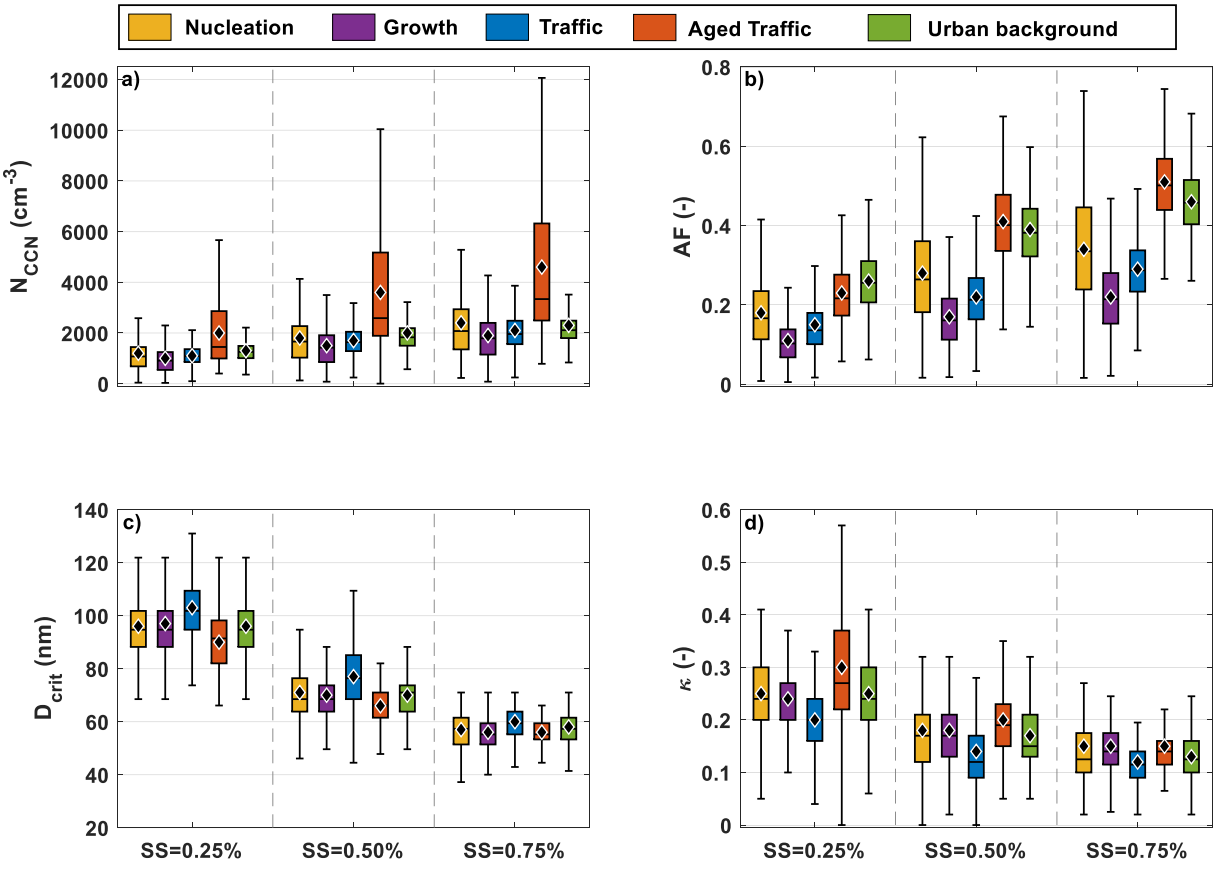

Fig. 4. Box-Whisker representation for CCN concentration, activation fraction (AF), critical diameter (D_{crit}), and kappa parameter (κ) at SS = 0.25, 0.50 and 0.75 % for the different aerosol population categories. The black diamonds represent the mean values for each parameter.

In Fig. 5, we show the probability density function (PDF) of N_{CCN} data at the three selected SS. All CCN PDFs have a unimodal distribution for all SS values, except for the growth category which has two modes. In addition, there is a little second mode at larger N_{CCN} concentration in the aged traffic category. The traffic and urban background categories have the narrowest distributions at all SS indicating that N_{CCN} is constrained to a limited range of values in this aerosol category (Fig. 5). Fig. 5 also shows that although the traffic category encompasses different traffic clusters, which have different PNSD as mentioned in the previous section, the narrow CCN PDF suggests that all traffic clusters have a similar contribution to the CCN concentration at all SS values.

The CCN PDF of the nucleation and growth aerosol categories have a similar shape with a wide distribution that includes low values of N_{CCN}. Therefore, the contribution of these aerosol categories to the CCN concentration was variable during the measurement period in contrast to the contribution of the urban background and traffic aerosol categories which was more constant. The CCN PDFs for the nucleation and growth clusters is wider because their hourly frequency distributions vary by month, due to the temporal variation of the aerosol properties and atmospheric conditions. Both the growth and nucleation categories have a ceiling value of N_{CCN} of around 1000 cm^{-3} at SS = 0.25 %. Assuming that most freshly nucleated particles are not able to activate, the CCN PDF mode of the nucleation category could be associated with the background aerosols. However, since the nucleation and growth categories exhibit similar CCN PDFs at all SS (Fig. 5), we assume that the growth category is associated with the same origin as the nucleation category.

Lastly, the aged traffic category represents an intermediate situation in terms of the CCN PDF width with respect to the abovementioned cases. Its distribution neither is constrained to a limited range of N_{CCN} (as is the case of the traffic and urban background categories) nor exhibits a clear skewness to low values of N_{CCN} (i.e., nucleation and growth categories). The aged traffic CCN PDF has a primary mode at 1038 cm^{-3} at SS = 0.25 % and shows some skewness to higher values of N_{CCN} (e.g., the secondary mode at 3131 cm^{-3} at SS = 0.25 %). Thus, the second mode of the PDF associated with higher N_{CCN} reveals some specific conditions in which the ageing of traffic emissions could be more efficient at this urban site.

4.2.2. Critical diameter (D_{crit})

The mean D_{crit} values range from 70 nm to 130 nm at SS = 0.25 %, from 45 to 100 nm at SS = 0.50 % and from 30 to 75 nm at SS = 0.75 %. The D_{crit} values and variability decrease with supersaturation for all aerosol categories (Fig. 5). The D_{crit} for the nucleation category ranges from 96 nm at 0.25 % to 57 nm at 0.75 %. D_{crit} for the growth category shows very similar values as nucleation category (from 97 nm at 0.25 % to 56 nm at 0.75 %). Also, the change of this value when increasing the SS values is similar (Table 2) and this fact is related to the similar PNSD shape in the range defined by the D_{crit} for both aerosol categories (between 60 and 100 nm, see Fig. 3). For the traffic category, D_{crit} values ranges from 103 nm to 60 nm from the lowest to the highest SS, being the largest values of all categories (Table 2). This fact is consistent with the known non-hygroscopic behavior of traffic particles and explains why the traffic N_{CCN} is lower than the nucleation/growth values even though traffic PNSD presents higher concentration above 80 nm. On the other hand, aged traffic values range from 90 nm at SS = 0.25 % to 56 nm at SS = 0.75 %. These D_{crit} values coincide with the particle diameter range where aged traffic PNSD shows its maximum (Fig. 3). The urban background category presents D_{crit} values ranging from 96 ± 10 nm at SS = 0.25 % to 58 ± 6 nm at SS = 0.75 % and shows a similar behavior with SS as the rest of aerosol categories (Fig. 4). Therefore, there are not remarkable differences in D_{crit} among aerosol categories. This is explained by the similarities in the PNSD in the diameter range between 60 and 500 nm among all aerosol categories, except for the aged traffic category. The D_{crit} values are similar to other urban sites (influenced by traffic

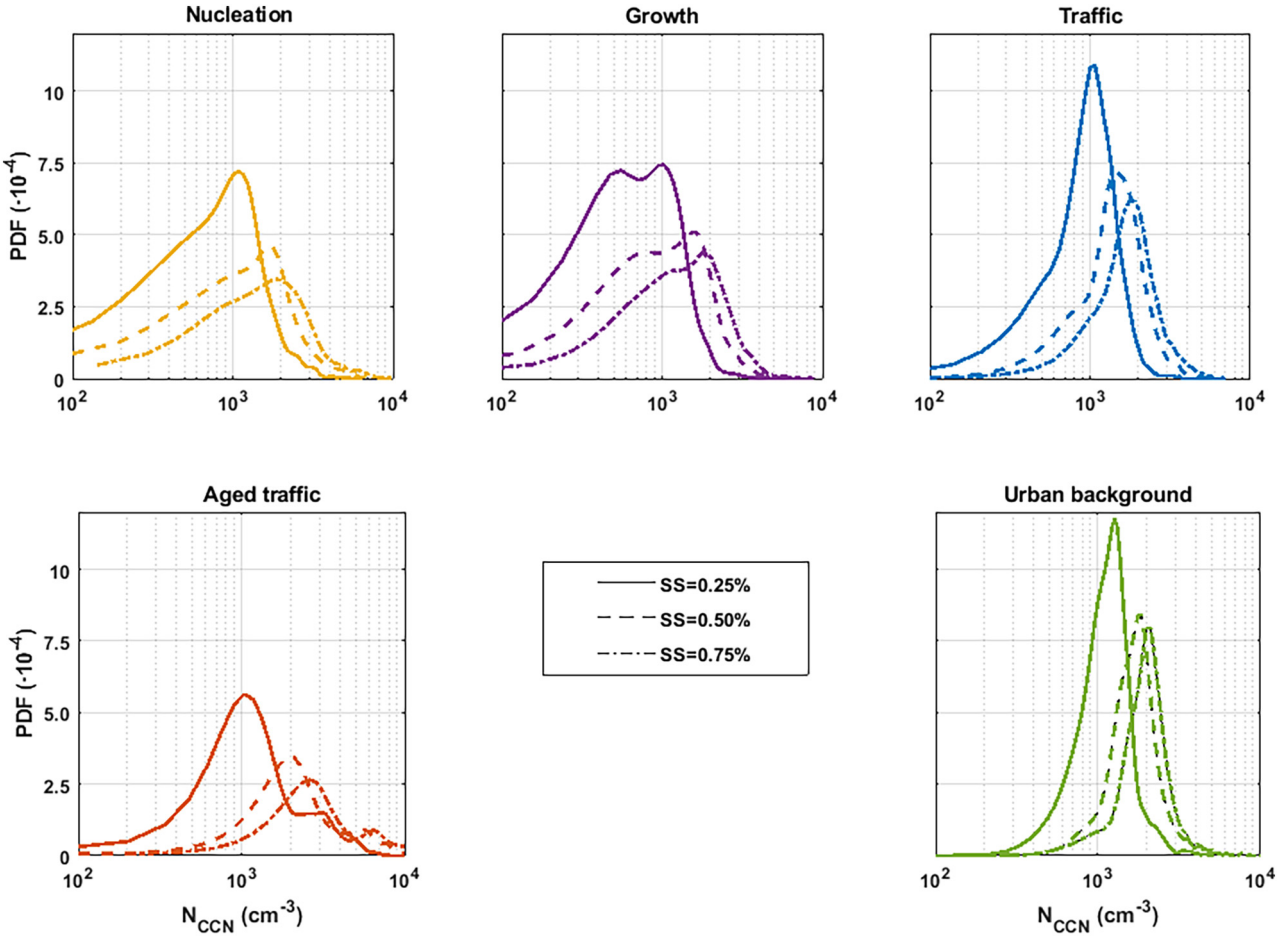

Fig. 5. Probability density function (PDF) of the CCN concentration at different SS values associated to each aerosol population type.

activity, nucleation or aged pollution) reporting D_{crit} values ranging from 50 nm at high SS to 100 nm at low SS (Gunthe et al., 2011; Jurányi et al., 2013; Rejano et al., 2021; Salma et al., 2021).

4.2.3. Activation fraction (AF)

The activation parameter that better describes the activation capacity of each aerosol category type is the AF because it provides information about the relative contribution of the whole PNSD to the CCN concentration. Based on the PNSD showed in Fig. 3 and the mentioned D_{crit} values, AF mean values remain below 0.5 for all aerosol categories at all SS, except for the aged traffic category at SS = 0.75 % (Table 2). From the lowest to the highest SS, mean AF values range from 0.11 up to 0.51. In Fig. 4 we can observe that the dispersion of AF values (the width of the boxplot) is approximately constant along the different aerosol categories because the variability in N_{CCN} is compensated by the variability in N_{tot}. AF values for growth and traffic categories are the lowest and do not exceed 0.30 even at high SS. In fact AF values for the traffic category agree with those reported at traffic influenced sites during traffic rush hours (e.g., Burkart et al., 2011; Cubison et al., 2008; Rejano et al., 2021). These low AF values are related to the high concentration of particles below 20 nm and the low concentration above 70 nm. Note that nucleation category presents higher AF values than growth and traffic categories which can be explained by the noticeable particle concentration above 70 nm observed in nucleation category (Fig. 3). On the contrary, the aged traffic and urban background categories have the highest AF values. Also, the increase in AF when increasing SS value is more noticeable in the aged traffic and urban background categories than on the other categories. The diurnal timing of the aged traffic category coincides with the hours that Rejano et al. (2021) observed the maximum value of the AF during the day at this site. Also, the AF values for the urban background category are high compared to the other categories since the urban background category PNSD is strongly influenced by accumulation particles.

At SS = 0.25 % we observe that AF is between 0.15, while at SS = 0.50 % the AF is 0.25 which is just a quarter of the total particle number concentration that activates as CCN. Those values are typical for urban environments at low and medium SS values (Salma et al., 2021). However, the aged traffic and urban background categories achieve AF values around 0.4 at SS = 0.50 %, similar to the AF mean values for different regional and remote sites analyzed in Paramonov et al. (2015). Moreover, the AF values of the aged traffic and urban background categories are consistent with the AF values identified during the CalWater-2015 field campaign, with AF ranging from 0.2 to 0.6 for SS from 0.2 % to 0.7 % (Atwood et al., 2019). In the cited study one cluster was identified as a mixed cluster of freshly emitted aerosols or new particle formation event, whose AF values for the SS values between 0.2 and 0.5 % were in the range of 0.15–0.20.

4.2.4. Hygroscopicity parameter (κ)

The hygroscopicity parameter shows a wide range of values for the different aerosol categories. In Fig. 4 we can observe a decrease of κ value and its range of variability for all aerosol categories when the SS increases (as occurs with D_{crit}). The mean κ parameter values mainly remain below 0.4 and above 0.1 for all SS and shows similar mean values along the aerosol categories (Table 2). In the case of the nucleation and growth category, κ shows an identical behavior and ranges from 0.25 at SS = 0.25 % to 0.15 at SS = 0.75 %. Traffic category presents the lowest κ which is expected due to the hydrophobic chemical composition associated to fresh traffic emissions. On the other hand, aged traffic and urban background

categories have the highest κ values across all aerosol categories at low SS, whereas at high SS all categories present very similar values.

We must consider that the effective hygroscopicity parameter provides indirect information about the hygroscopicity of particles around the D_{crit}. Therefore, depending on the SS value at which the D_{crit} was obtained, the particle hygroscopicity is associated with different particle size ranges. According to the D_{crit} values obtained at the different SS values (around 100 nm at SS = 0.25 % and 55 nm at SS = 0.75 %), κ values could be associated with accumulation mode at SS = 0.25 % and aged Aitken mode particles at SS = 0.50 and 0.75 %. Thus, our results suggest that smaller particles (related to Aitken mode particles) are less hygroscopic than larger ones (related to accumulation mode particles). In the case of accumulation mode particles all aerosol categories exhibit similar κ values (ranging from 0.2 to 0.30), which is consistent with the results of Cai et al. (2018) for the Guangzhou region in China. They observed that κ for particles around 100 nm has values between 0.2 and 0.3 using different methodologies, including assessing hygroscopic growth with a HTDMA, applying a chemical composition approach using an AMS and using a CCNc at SS = 0.20 %. In our study, the two aerosols categories which are related to aged particles have the highest κ values.

Also, we can observe in Fig. 4 that the hygroscopicity parameter present a similar behavior as N_{CCN} for all the aerosol categories. Note that the variability (width of the box) of N_{CCN} and κ are similar for each aerosol type, except for the aged traffic category which presents the highest variability in κ and N_{CCN}. Thus, this variability suggests that different ageing processes may lead to higher or lower values of the hygroscopicity parameter (up to a maximum value of 0.45), with CCN concentrations of up to 4000 cm^{-3} at SS = 0.25 %. The κ parameter for aged traffic category exhibits the highest values of all aerosol populations, confirming our hypothesis that aged traffic particles undergo ageing processes like oxidation due to photochemical reactions. Many studies have investigated the influence that the oxidation level of organic aerosols has on the increase of κ parameter at urban environments (e.g., Kuang et al., 2020; Wu et al., 2016).

5. Summary and conclusions

In this study, the PNSD in the size range between 4 and 500 nm and CCN concentrations at various supersaturations (SS) were measured at an urban background site in southern Europe. An unsupervised model based on a k-means algorithm was used to group data according to their PNSD with the aim of identifying urban aerosol sources and processes. The classification resulted in 10 clusters which explain the aerosol population variability during the studied period. According to additional analysis, the different clusters were associated with different aerosol categories: three clusters account for traffic emissions, two clusters for freshly nucleated particles, three for growth particles after NPF events, one for aged traffic emissions and one for urban background particles. The unsupervised classification showed that traffic emissions and NPF events, including freshly nucleated particles and first stage growth particles, are the most frequent aerosol category in this urban environment during the analyzed period, representing around the 80 % of the whole dataset. Moreover, in this study we suggest an important process to consider at urban environments, which is the ageing undergone by aerosol particles from traffic emissions. This aerosol category is observed over a very limited period (only represents the 8 % of the dataset) but such ageing can have important implications for the transformations that aerosol particles undergo in an urban environment and determine their ability to act as CCN.

Once the different aerosol categories were identified, we characterized their activation properties to evaluate their influence on the CCN budget. Results showed that aged traffic particles have the largest influence on the CCN concentration for all SS values, whereas the other four aerosol types had a more limited influence on CCN concentration because of their different properties and origin. The nucleation and growth categories had similar contribution to CCN (albeit lower than the aged traffic category), indicating that a further growth/processing is required to observe a relevant effect of NPF events on CCN concentrations since growth category barely increases the nucleation contribution. The AF, which accounts for the activation efficiency of each aerosol population, showed the highest values for the urban background and aged traffic categories and the lowest for growth and traffic categories, demonstrating the key role of particle size in the activation of particles as CCN. The differences in AF values among aerosol types increased at higher SS values, revealing the differences that exist among the PNSDs. Thus, our results allow to constrain the AF values for all aerosol categories between 0.22 (for growth category) and 0.51 (aged traffic category) at SS = 0.75 %. In this sense, we estimate CCN-active size range for each urban aerosol categories: D_{crit} ranges along aerosol categories 90–100 nm at SS = 0.25 %, 65–80 nm at 0.50 % and 56–60 at SS = 0.75 %. Related to the hygroscopicity of particles, all aerosol categories show κ values around 0.15–0.30. The traffic category had the lowest κ value as is expected due to the hydrophobic behavior of BC particles dominating these traffic emissions. However, our results indicated that these particles become more hygroscopic after ageing. The κ for the aged traffic category suggested that these particles had different chemical composition than fresh traffic particles, as well as different size. In this study we have constrained the activation parameters for the main aerosol categories in an urban, which could be extended to other urban sites around the world, which help to reduce the uncertainty associated to the CCN concentrations in a regional scale.

To conclude, this study highlights the indirect effect of traffic emissions on the CCN concentration. Traffic emissions in urban environment are known to have an important impact on the aerosol population due to their high number concentration, but the direct influence of traffic emissions on the CCN budget is limited. However, when these particles undergo ageing, they could have a significant impact on the CCN concentration (even at low SS values) and may be an important CCN source in urban environments, especially at sites close to high-altitude areas where aerosol is efficiently transported to higher atmospheric layers. In this sense, aged traffic particles could be transported to other environments where clouds form, triggering a plausible indirect effect of traffic emission on aerosol-cloud interactions which, to our knowledge, have not previously been considered.

CRediT authorship contribution statement

F. Rejano: Conceptualization, Investigation, Methodology, Data curation, Writing – original draft, Visualization. **J.A. Casquero-Vera:** Data curation, Formal analysis, Writing – review & editing. **H. Lyamani:** Conceptualization, Resources, Investigation. **E. Andrews:** Writing – review & editing. **A. Casans:** Data curation, Visualization. **D. Pérez-Ramírez:** Writing – review & editing. **L. Alados-Arboledas:** Supervision, Funding acquisition. **G. Titos:** Conceptualization, Investigation, Methodology, Project administration, Writing – review & editing, Funding acquisition. **F.J. Olmo:** Supervision, Project administration, Writing – review & editing, Funding acquisition.

Data availability

The authors are unable or have chosen not to specify which data has been used.

Declaration of competing interest

The authors declare that they have no known competing financial interests or personal relationships that could have appeared to influence the work reported in this paper.

Acknowledgments

This work was supported by BioCloud project (RTI2018.101154.A.I00) funded by MCIN/AEI/ 10.13039/501100011033 and FEDER “Una manera de hacer Europa”, by the European Union's Horizon 2020 research and innovation program through project ACTRIS.IMP (grant agreement No 871115) and ATMO_ACCESS (grant agreement No 101008004), by the

Spanish Ministry of Science and Innovation through projects ELPIS (PID2020-12001-5RB-I00), CLARIN (CGL2016-81092-R) and ACTRIS-España (CGL2017-90884REDT), by Junta de Andalucía, UGR and FEDER funds through project B-RNM-474-UGR18 and NIMBUS (B-RNM-496-UGR18), by the Junta de Andalucía Excellence project ADAPNE (P20-00136), AEROPRE (P-18-RT-3820) and by University of Granada Plan Propio through Visiting Scholars (PPVS2018-04) and Singular Laboratory (LS2022-1) programs. Fernando Rejano is funded by Spanish Ministry of Universities through predoctoral grant FPU19/05340. Andrea Casans is funded by Spanish Ministry of Research and Innovation under the predoctoral program FPI (PRE2019-090827). Thanks to the NOAA Global Monitoring Laboratory for providing the data acquisition and processing system and for the use of the CCN counter.

Appendix A. Supplementary data

Supplementary data to this article can be found online at https://doi.org/10.1016/j.scitotenv.2022.159657.

References

Agudelo-Castañeda, D.M., Teixeira, E.C., Braga, M., Rolim, S.B.A., Silva, L.F.O., Beddows, D.C.S., Harrison, R.M., Querol, X., 2019. Cluster analysis of urban ultrafine particles size distributions. Atmos. Pollut. Res. 10 (1), 45–52. https://doi.org/10.1016/J.APR.2018.06.006.

Andreae, M.O., Rosenfeld, D., 2008. Part 1. The nature and sources of cloud-active aerosols. Earth-Science Rev. 89 (1–2), 13–41. https://doi.org/10.1016/j.earscirev.2008.03.001.

Andrews, E., Sheridan, P.J., Ogren, J.A., Hageman, D., Jefferson, A., Wendell, J., Alástuey, A., Alados-Arboledas, L., Bergin, M., Ealo, M., Sorribas, M., Sun, J., 2019. Overview of the NOAA/ESRL federated aerosol network. Bull. Am. Meteorol. Soc. 100 (1), 123–135. https://doi.org/10.1175/BAMS-D-17-0175.1.

Arbelaitz, O., Gurrutxaga, I., Muguerza, J., Pérez, J.M., Perona, I., 2013. An extensive comparative study of cluster validity indices. Pattern Recogn. 46 (1), 243–256. https://doi.org/10.1016/j.patcog.2012.07.021.

Atwood, S.A., Reid, J.S., Kreidenweis, S.M., Blake, D.R., Jonsson, H.H., Lagrosas, N.D., Xian, P., Reid, E.A., Sessions, W.R., Simpas, J.B., 2017. Size-resolved aerosol and cloud condensation nuclei (CCN) properties in the remote marine South China Sea – part 1: observations and source classification. Atmos. Chem. Phys. 17 (2), 1105–1123. https://doi.org/10.5194/acp-17-1105-2017.

Atwood, S.A., Kreidenweis, S.M., DeMott, P.J., Petters, M.D., Cornwell, G.C., Martin, A.C., Moore, K.A., 2019. Classification of aerosol population type and cloud condensation nuclei properties in a coastal California littoral environment using an unsupervised cluster model. Atmos. Chem. Phys. 19 (10), 6931–6947. https://doi.org/10.5194/acp-19-6931-2019.

Beddows, D.C.S., Dall'Osto, M., Harrison, R., 2009. M.: cluster analysis of rural, urban, and curbside atmospheric particle size data. Environ. Sci. Technol. 43 (13), 4694–4700. https://doi.org/10.1021/es803121t.

Beddows, D.C.S., Harrison, R.M., Green, D.C., Fuller, G.W., 2015. Receptor modelling of both particle composition and size distribution from a background site in London, UK. Atmos. Chem. Phys. 15, 10107–10125. https://doi.org/10.5194/acp-15-10107-2015.

Bougiatioti, A., Nenes, A., Lin, J.J., Brock, C.A., de Gouw, J.A., Liao, J., Middlebrook, A.M., Welti, A., 2020. Drivers of cloud droplet number variability in the summertime in the southeastern United States. Atmos. Chem. Phys. 20 (20), 12163–12176. https://doi.org/10.5194/acp-20-12163-2020.

Brines, M., Dall'Osto, M., Beddows, D.C.S., Harrison, R.M., Querol, X., 2014. Simplifying aerosol size distributions modes simultaneously detected at four monitoring sites during SAPUSS. Atmos. Chem. Phys. 14 (6), 2973–2986. https://doi.org/10.5194/acp-14-2973-2014.

Brines, M., Dall'Osto, M., Beddows, D.C.S., Harrison, R.M., Gómez-Moreno, F., Núñez, L., Artíñano, B., Costabile, F., Gobbi, G.P., Salimi, F., Morawska, L., Sioutas, C., Querol, X., 2015. Traffic and nucleation events as main sources of ultrafine particles in high-insolation developed world cities. Atmos. Chem. Phys. 15 (10), 5929–5945. https://doi.org/10.5194/acp-15-5929-2015.

Burkart, J., Steiner, G., Reischl, G., Hitzenberger, R., 2011. Long-term study of cloud condensation nuclei (CCN) activation of the atmospheric aerosol in Vienna. Atmos. Environ. https://doi.org/10.1016/j.atmosenv.2011.07.022.

Cai, M., Liang, B., Sun, Q., Zhou, S., Chen, X., Yuan, B., Shao, M., Tan, H., Zhao, J., 2020. Effects of continental emissions on cloud condensation nuclei (CCN) activity in the northern South China Sea during summertime 2018. Atmos. Chem. Phys. 20, 9153–9167. https://doi.org/10.5194/acp-20-9153-2020.

Cai, M., Tan, H., Chan, C.K., Qin, Y., Xu, H., Li, F., Schurman, M.I., Liu, L., Zhao, J., 2018. The size-resolved cloud condensation nuclei (CCN) activity and its prediction based on aerosol hygroscopicity and composition in the Pearl Delta River (PRD) region during wintertime, 2014. Atmos. Chem. Phys. 18 (22). https://doi.org/10.5194/acp-18-16419-2018.

Casquero-Vera, J.A., Lyamani, H., Titos, G., Borrás, E., Olmo, F.J., Alados-Arboledas, L., 2019. Impact of primary NO2 emissions at different urban sites exceeding the european NO2 standard limit. Sci. Total Environ. 646, 1117–1125. https://doi.org/10.1016/j.scitotenv.2018.07.360.

Casquero-Vera, J.A., Lyamani, H., Dada, L., Hakala, S., Paasonen, P., Román, R., Fraile, R., Petäjä, T., Olmo-Reyes, F.J., Alados-Arboledas, L., 2020. New particle formation at urban and high-altitude remote sites in the South-Eastern Iberian Peninsula. Atmos. Chem. Phys. 20 (22), 14253–14271. https://doi.org/10.5194/acp-20-14253-2020.

Casquero-Vera, J.A., Lyamani, H., Titos, G., Minguillón, M.C., Dada, L., Alastuey, A., Querol, X., Petäjä, T., Olmo, F.J., Alados-Arboledas, L., 2021. Quantifying traffic, biomass burning and secondary source contributions to atmospheric particle number concentrations at urban and suburban sites. Sci. Total Environ. 768. https://doi.org/10.1016/j.scitotenv.2021.145282.

Casquero-Vera, J.A., Lyamani, H., Titos, G., Moreira, G.D.A., Benavent-Oltra, J.A., Conte, M., Contini, D., Järvi, L., Olmo-Reyes, F.J., Alados-Arboledas, L., 2022. Aerosol number fluxes and concentrations over a southern european urban area. Atmos. Environ. 269. https://doi.org/10.1016/j.atmosenv.2021.118849.

Charron, A., Birmili, W., Harrison, R.M., 2008. Fingerprinting particle origins according to their size distribution at a UK rural site. J. Geophys. Res. 113 (D7), D07202. https://doi.org/10.1029/2007JD008562.

Cheung, H.C., Chou, C.C.-K., Lee, C.S.L., Kuo, W.-C., Chang, S.-C., 2020. Hygroscopic properties and cloud condensation nuclei activity of atmospheric aerosols under the influences of asian continental outflow and new particle formation at a coastal site in eastern Asia. Atmos. Chem. Phys. 20 (10), 5911–5922. https://doi.org/10.5194/acp-20-5911-2020.

Costabile, F., Birmili, W., Klose, S., Tuch, T., Wehner, B., Wiedensohler, A., Franck, U., König, K., Sonntag, A., 2009. Spatio-temporal variability and principal components of the particle number size distribution in an urban atmosphere. Atmos. Chem. Phys. 9 (9), 3163–3195. https://doi.org/10.5194/acp-9-3163-2009.

Crilley, L.R., Lucarelli, F., Bloss, W.J., Harrison, R.M., Beddows, D.C., Calzolai, G., Nava, S., Valli, G., Bernardoni, V., Vecchi, R., 2017. Source apportionment of fine and coarse particles at a roadside and urban background site in London during the 2012 summer ClearfLo campaign. Environ. Pollut. 220, 766–778. https://doi.org/10.1016/J.ENVPOL.2016.06.002.

Crosbie, E., Youn, J.-S., Balch, B., Wonaschütz, A., Shingler, T., Wang, Z., Conant, W.C., Betterton, E.A., Sorooshian, A., 2015. On the competition among aerosol number, size and composition in predicting CCN variability: a multi-annual field study in an urbanized desert. Atmos. Chem. Phys. 15 (12), 6943–6958. https://doi.org/10.5194/acp-15-6943-2015.

Cubison, M.J., Ervens, B., Feingold, G., Docherty, K.S., Ulbrich, I.M., Shields, L., Prather, K., Hering, S., Jimenez, J.L., 2008. The influence of chemical composition and mixing state of Los Angeles urban aerosol on CCN number and cloud properties. Atmos. Chem. Phys. 8 (18), 5649–5667. https://doi.org/10.5194/acp-8-5649-2008.

Dall'Osto, M., Monahan, C., Greaney, R., Beddows, D.C.S., Harrison, R.M., Ceburnis, D., O'Dowd, C., 2011. D.: a statistical analysis of north East Atlantic (submicron) aerosol size distributions. Atmos. Chem. Phys. 11 (24), 12567–12578. https://doi.org/10.5194/acp-11-12567-2011.

Davies, D.L., Bouldin, D., 1979. W.: a cluster separation measure. IEEE Trans. Pattern Anal. Mach. Intell. PAMI-1(2), 224–227. https://doi.org/10.1109/TPAMI.1979.4766909.

del Águila, A., Sorribas, M., Lyamani, H., Titos, G., Olmo, F.J., Arruda-Moreira, G., Yela, M., Alados-Arboledas, L., 2018. Sources and physicochemical characteristics of submicron aerosols during three intensive campaigns in Granada (Spain). Atmos. Res. 213, 398–410. https://doi.org/10.1016/j.atmosres.2018.06.004.

Dusek, U., Frank, G.P., Hildebrandt, L., Curtius, J., Schneider, J., Walter, S., Chand, D., Drewnick, F., Hings, S., Jung, D., Borrmann, S., Andreae, M.O., 2006. Size matters more than chemistry for cloud-nucleating ability of aerosol particles. Science 80-.), 312(5778, 1375–1378. https://doi.org/10.1126/science.1125261.

Gentner, D.R., Isaacman, G., Worton, D.R., Chan, A.W.H., Dallmann, T.R., Davis, L., Liu, S., Day, D.A., Russell, L.M., Wilson, K.R., Weber, R., Guha, A., Harley, R.A., Goldstein, A., 2012. H.: elucidating secondary organic aerosol from diesel and gasoline vehicles through detailed characterization of organic carbon emissions. Proc. Natl. Acad. Sci. U. S. A. 109 (45), 18318–18323. https://doi.org/10.1073/pnas.1212272109.

Gunthe, S.S., Rose, D., Su, H., Garland, R.M., Achtert, P., Nowak, A., Wiedensohler, A., Kuwata, M., Takegawa, N., Kondo, Y., Andreae, M.O., Pöschl, U., 2011. Cloud condensation nuclei (CCN) from fresh and aged air pollution in the megacity region of Beijing. Atmos. Chem. Phys. 11 (21), 11023–11039. https://doi.org/10.5194/acp-11-11023-2011.

Intergovernmental Panel on Climate Change (IPCC), 2021Intergovernmental Panel on Climate Change (IPCC): IPCC: Climate Change 2021: The Physical Science Basis. [online] Available from: https://www.ipcc.ch/report/ar6/wg1/, 2021.

Jurányi, Z., Tritscher, T., Gysel, M., Laborde, M., Gomes, L., Roberts, G., Baltensperger, U., Weingartner, E., 2013. Hygroscopic mixing state of urban aerosol derived from size-resolved cloud condensation nuclei measurements during the MEGAPOLI campaign in Paris. Atmos. Chem. Phys. 13 (13), 6431–6446. https://doi.org/10.5194/acp-13-6431-2013.

Jurányi et al., 2011. Jurányi, Z., Gysel, M., Weingartner, E., Bukowiecki, N., Kammermann, L. and Baltensperger, U.: A 17 month climatology of the cloud condensation nuclei number concentration at the high alpine site Jungfraujoch, J. Geophys. Res. Atmos., 116(10), doi: 10.1029/2010JD015199, 2011.

Kroll, J.H., Seinfeld, J.H., 2008. Chemistry of secondary organic aerosol: formation and evolution of low-volatility organics in the atmosphere. Atmos. Environ. 42 (16), 3593–3624. https://doi.org/10.1016/j.atmosenv.2008.01.003.

Kruskal, W.H., Wallis, W., 1952. A.: use of ranks in one-criterion variance analysis. J. Am. Stat. Assoc. 47, 583–621. https://doi.org/10.2307/2280779.

Kuang, Y., He, Y., Xu, W., Zhao, P., Cheng, Y., Zhao, G., Tao, J., Ma, N., Su, H., Zhang, Y., Sun, J., Cheng, P., Yang, W., Zhang, S., Wu, C., Sun, Y., Zhao, C., 2020. Distinct diurnal variation in organic aerosol hygroscopicity and its relationship with oxygenated organic aerosol. Atmos. Chem. Phys. 20 (2), 865–880. https://doi.org/10.5194/acp-20-865-2020.

Lee, Y., Choi, Y., An, H., Park, J., Ghim, Y.S., 2021. Cluster analysis of atmospheric particle number size distributions at a rural site downwind of Seoul, Korea. Atmos. Pollut. Res. 12 (6), 101086. https://doi.org/10.1016/J.APR.2021.101086.

Liang, C.-S., Yue, D., Wu, H., Shi, J.-S., He, K.-B., 2021. Source apportionment of atmospheric particle number concentrations with wide size range by nonnegative matrix factorization (NMF). Environ. Pollut. 289. https://doi.org/10.1016/j.envpol.2021.117846.

Lyamani, H., Olmo, F.J., Alados-Arboledas, L., 2005. Saharan dust outbreak over southeastern Spain as detected by sun photometer. Atmos. Environ. 39 (38), 7276–7284. https://doi.org/10.1016/j.atmosenv.2005.09.011.

Lyamani, H., Olmo, F.J., Foyo, I., Alados-Arboledas, L., 2011. Black carbon aerosols over an urban area in South-Eastern Spain: changes detected after the 2008 economic crisis. Atmos. Environ. 45 (35), 6423–6432. https://doi.org/10.1016/j.atmosenv.2011.07.063.

Lyamani, H., Fernández-Gálvez, J., Pérez-Ramírez, D., Valenzuela, A., Antón, M., Alados, I., Titos, G., Olmo, F.J., Alados-Arboledas, L., 2012. Aerosol properties over two urban sites in South Spain during an extended stagnation episode in winter season. Atmos. Environ. 62, 424–432. https://doi.org/10.1016/j.atmosenv.2012.08.050.

Müller, T., Henzing, J.S., de Leeuw, G., Wiedensohler, A., Alastuey, A., Angelov, H., Bizjak, M., Collaud Coen, M., Engström, J.E., Gruening, C., Hillamo, R., Hoffer, A., Imre, K., Ivanow, P., Jennings, G., Sun, J.Y., Kalivitis, N., Karlsson, H., Komppula, M., Laj, P., Li, S.-M., Lunder, C., Marinoni, A., Martins dos Santos, S., Moerman, M., Nowak, A., Ogren, J.A., Petzold, A., Pichon, J.M., Rodriquez, S., Sharma, S., Sheridan, P.J., Teinilä, K., Tuch, T., Viana, M., Virkkula, A., Weingartner, E., Wilhelm, R., Wang, Y., 2011. Q.: characterization and intercomparison of aerosol absorption photometers: result of two intercomparison workshops. Atmos. Meas. Tech. 4 (2), 245–268. https://doi.org/10.5194/amt-4-245-2011.

Pandolfi, M., Alados-Arboledas, L., Alastuey, A., Andrade, M., Angelov, C., Artiñano, B., Backman, J., Baltensperger, U., Bonasoni, P., Bukowiecki, N., Wiedensohler, A., Laj, P., 2018. A european aerosol phenomenology - 6: scattering properties of atmospheric aerosol particles from 28 ACTRIS sites. Atmos. Chem. Phys. 18 (11), 7877–7911. https://doi.org/10.5194/acp-18-7877-2018.

Paramonov, M., Kerminen, V.-M., Gysel, M., Aalto, P.P., Andreae, M.O., Asmi, E., Baltensperger, U., Bougiatioti, A., Brus, D., Frank, G.P., Good, N., Gunthe, S.S., Hao, L., Irwin, M., Jaatinen, A., Jurányi, Z., King, S.M., Kortelainen, A., Kristensson, A., Lihavainen, H., Kulmala, M., Lohmann, U., Martin, S.T., McFiggans, G., Mihalopoulos, N., Nenes, A., O'Dowd, C.D., Ovadnevaite, J., Petäjä, T., Pöschl, U., Roberts, G.C., Rose, D., Svenningsson, B., Swietlicki, E., Weingartner, E., Whitehead, J., Wiedensohler, A., Wittbom, C., Sierau, B., 2015. A synthesis of cloud condensation nuclei counter (CCNC) measurements within the EUCAARI network. Atmos. Chem. Phys. 15 (21), 12211–12229. https://doi.org/10.5194/acp-15-12211-2015.

Pérez-Ramírez, D., Lyamani, H., Smirnov, A., Óneill, N.T., Veselovskii, I., Whiteman, D.N., Olmo, F.J., Alados-Arboledas, L., 2016. Statistical study of day and night hourly patterns of columnar aerosol properties using sun and star photometry. Proceedings of SPIE - The International Society for Optical Engineering 10001.

Petters, M.D., Kreidenweis, S.M., 2007. A single parameter representation of hygroscopic growth and cloud condensation nucleus activity. Atmos. Chem. Phys. 7 (8), 1961–1971. https://doi.org/10.5194/acp-7-1961-2007.

Rejano, F., Titos, G., Casquero-Vera, J.A., Lyamani, H., Andrews, E., Sheridan, P., Cazorla, A., Castillo, S., Alados-Arboledas, L., Olmo, F.J., 2021. Activation properties of aerosol particles as cloud condensation nuclei at urban and high-altitude remote sites in southern Europe. Sci. Total Environ. 762, 143100. https://doi.org/10.1016/j.scitotenv.2020.143100.

Ripamonti, G., Järvi, L., Mølgaard, B., Hussein, T., Nordbo, A., Hämeri, K., 2013. The effect of local sources on aerosol particle number size distribution, concentrations and fluxes in Helsinki, Finland, tellus. Ser. B Chem. Phys. Meteorol. 65 (1). https://doi.org/10.3402/tellusb.v65i0.19786.

Rivas, I., Beddows, D.C.S., Amato, F., Green, D.C., Järvi, L., Hueglin, C., Reche, C., Timonen, H., Fuller, G.W., Niemi, J.V., Pérez, N., Aurela, M., Hopke, P.K., Alastuey, A., Kulmala, M., Harrison, R.M., Querol, X., Kelly, F.J., 2020. Source apportionment of particle number size distribution in urban background and traffic stations in four european cities. Environ. Int. 135, 105345. https://doi.org/10.1016/j.envint.2019.105345.

Robinson, A.L., Donahue, N.M., Shrivastava, M.K., Weitkamp, E.A., Sage, A.M., Grieshop, A.P., Lane, T.E., Pierce, J.R., Pandis, S.N., 2007. Rethinking organic aerosols: semivolatile emissions and photochemical aging. Science 80-.), 315(5816, 1259–1262. https://doi.org/10.1126/science.1133061.

Rodríguez, S., Cuevas, E., 2007. The contributions of "minimum primary emissions" and "new particle formation enhancements" to the particle number concentration in urban air. J. Aerosol Sci. 38 (12), 1207–1219. https://doi.org/10.1016/j.jaerosci.2007.09.001.

Rönkkö, T., Kuuluvainen, H., Karjalainen, P., Keskinen, J., Hillamo, R., Niemi, J.V., Pirjola, L., Timonen, H.J., Saarikoski, S., Saukko, E., Järvinen, A., Silvennoinen, H., Rostedt, A., Olin, M., Yli-Ojanperä, J., Nousiainen, P., Kousa, A., Dal Maso, M., 2017. Traffic is a major source of atmospheric nanocluster aerosol. Proc. Natl. Acad. Sci. U. S. A. 114 (29), 7549–7554. https://doi.org/10.1073/pnas.1700830114.

Rose, C., Collaud Coen, M., Andrews, E., Lin, Y., Bossert, I., Lund Myhre, C., Tuch, T., Wiedensohler, A., Fiebig, M., Aalto, P., Alastuey, A., Alonso-Blanco, E., Andrade, M., Artíñano, B., Arsov, T., Baltensperger, U., Bastian, S., Bath, O., Beukes, J.P., Brem, B.T., Bukowiecki, N., Casquero-Vera, J.A., Conil, S., Eleftheriadis, K., Favez, O., Flentje, H., Gini, M.I., Gómez-Moreno, F.J., Gysel-Beer, M., Hallar, A.G., Kalapov, I., Kalivitis, N., Kasper-Giebl, A., Keywood, M., Kim, J.E., Kim, S.-W., Kristensson, A., Kulmala, M., Lihavainen, H., Lin, N.-H., Lyamani, H., Marinoni, A., Martins Dos Santos, S., Mayol-Bracero, O.L., Meinhardt, F., Merkel, M., Metzger, J.-M., Mihalopoulos, N., Ondracek, J., Pandolfi, M., Pérez, N., Petäjä, T., Petit, J.-E., Picard, D., Pichon, J.-M., Pont, V., Putaud, J.-P., Reisen, F., Sellegri, K., Sharma, S., Schauer, G., Sheridan, P., Sherman, J.P., Schwerin, A., Sohmer, R., Sorribas, M., Sun, J., Tulet, P., Vakkari, V., van Zyl, P.G., Velarde, F., Villani, P., Vratolis, S., Wagner, Z., Wang, S.-H., Weinhold, K., Weller, R., Yela, M., Zdimal, V., Laj, P., 2021. Seasonality of the particle number concentration and size distribution: a global analysis retrieved from the network of Global Atmosphere Watch (GAW) near-surface observatories. Atmos. Chem. Phys. 21 (22), 17185–17223. https://doi.org/10.5194/acp-21-17185-2021.

Salimi, F., Ristovski, Z., Mazaheri, M., Laiman, R., Crilley, L.R., He, C., Clifford, S., Morawska, L., 2014. Assessment and application of clustering techniques to atmospheric particle number size distribution for the purpose of source apportionment. Atmos. Chem. Phys. 14 (21), 11883–11892. https://doi.org/10.5194/acp-14-11883-2014.

Salma, I., Thén, W., Vörösmarty, M., Gyöngyösi, A.Z., 2021. Cloud activation properties of aerosol particles in a continental central european urban environment. Atmos. Chem. Phys. 21 (14), 11289–11302. https://doi.org/10.5194/acp-21-11289-2021.

Schmale, J., Henning, S., Decesari, S., Henzing, B., Keskinen, H., Sellegri, K., Ovadnevaite, J., Pöhlker, M., Brito, J., Bougiatioti, A., Baltensperger, U., Gysel, M., 2018. Long-term cloud condensation nuclei number concentration, particle number size distribution and chemical composition measurements at regionally representative observatories. Atmos. Chem. Phys. 18 (4), 2853–2881. https://doi.org/10.5194/acp-18-2853-2018.

Seinfeld, J.H., Bretherton, C., Carslaw, K.S., Coe, H., DeMott, P.J., Dunlea, E.J., Feingold, G., Ghan, S., Guenther, A.B., Kahn, R., Kraucunas, I., Kreidenweis, S.M., Molina, M.J., Nenes, A., Penner, J.E., Prather, K.A., Ramanathan, V., Ramaswamy, V., Rasch, P.J., Ravishankara, A.R., Rosenfeld, D., Stephens, G., Wood, R., 2016. Improving our fundamental understanding of the role of aerosol-cloud interactions in the climate system. Proc. Natl. Acad. Sci. U. S. A. 113 (21), 5781–5790. https://doi.org/10.1073/pnas.1514043113.

Titos, G., Lyamani, H., Pandolfi, M., Alastuey, A., Alados-Arboledas, L., 2014. Identification of fine (PM1) and coarse (PM10–1) sources of particulate matter in an urban environment. Atmos. Environ. 89, 593–602. https://doi.org/10.1016/j.atmosenv.2014.03.001.

Titos, G., Lyamani, H., Drinovec, L., Olmo, F.J., Močnik, G., Alados-Arboledas, L., 2015. Evaluation of the impact of transportation changes on air quality. Atmos. Environ. 114, 19–31. https://doi.org/10.1016/j.atmosenv.2015.05.027.

Titos, G., del Águila, A., Cazorla, A., Lyamani, H., Casquero-Vera, J.A., Colombi, C., Cuccia, E., Gianelle, V., Močnik, G., Alastuey, A., Olmo, F.J., Alados-Arboledas, L., 2017. Spatial and temporal variability of carbonaceous aerosols: assessing the impact of biomass burning in the urban environment. Sci. Total Environ. 578, 613–625. https://doi.org/10.1016/j.scitotenv.2016.11.007.

Tunved, P., Ström, J., Hansson, H.-C., 2004. An investigation of processes controlling the evolution of the boundary layer aerosol size distribution properties at the swedish background station aspvreten. Atmos. Chem. Phys. 4 (11/12), 2581–2592. https://doi.org/10.5194/acp-4-2581-2004.

Valenzuela, A., Olmo, F.J., Lyamani, H., Antón, M., Quirantes, A., Alados-Arboledas, L., 2012. Aerosol radiative forcing during african desert dust events (2005–2010) over southeastern Spain. Atmos. Chem. Phys. 12 (21), 10331–10351. https://doi.org/10.5194/acp-12-10331-2012.

Wegner, T., Hussein, T., Hämeri, K., Vesala, T., Kulmala, M., Weber, S., 2012. Properties of aerosol signature size distributions in the urban environment as derived by cluster analysis. Atmos. Environ. 61, 350–360. https://doi.org/10.1016/j.atmosenv.2012.07.048.

Wiedensohler, A., Birmili, W., Nowak, A., Sonntag, A., Weinhold, K., Merkel, M., Wehner, B., Tuch, T., Pfeifer, S., Fiebig, M., Fjäraa, A.M., Asmi, E., Sellegri, K., Depuy, R., Venzac, H., Villani, P., Laj, P., Aalto, P., Ogren, J.A., Swietlicki, E., Williams, P., Roldin, P., Quincey, P., Hüglin, C., Fierz-Schmidhauser, R., Gysel, M., Weingartner, E., Riccobono, F., Santos, S., Grüning, C., Faloon, K., Beddows, D., Harrison, R., Monahan, C., Jennings, S.G., Marinoni, A., Horn, H.-G., Keck, L., Jiang, J., Scheckman, J., McMurry, P.H., Deng, Z., Zhao, C.S., Moerman, M., Henzing, B., de Leeuw, G., Löschau, G., Bastian, S., Dowd, C.D., 2012. Mobility particle size spectrometers: harmonization of technical standards and data structure to facilitate high quality long-term observations of atmospheric particle number size distributions. Atmos. Meas. Tech. 5 (3), 657–685. https://doi.org/10.5194/amt-5-657-2012.

Wilks, D., 2019. S.: statistical methods in atmoshperic sciences. Stat. Methods Atmos. Sci. 617–668.

Wu, T., Boor, B.E., 2021. Urban aerosol size distributions: a global perspective. Atmos. Chem. Phys. 21 (11), 8883–8914. https://doi.org/10.5194/acp-21-8883-2021.

Wu, Z.J., Zheng, J., Shang, D.J., Du, Z.F., Wu, Y.S., Zeng, L.M., Wiedensohler, A., Hu, M., 2016. Particle hygroscopicity and its link to chemical composition in the urban atmosphere of Beijing, China, during summertime. Atmos. Chem. Phys. 16 (2), 1123–1138. https://doi.org/10.5194/acp-16-1123-2016.